Coupling of finite element and boundary integral methods: Motion of ellipsoidal capsules in simple shear flow

Anne-Virginie Salsac, Johann Walter, Dominique Barthès-Biesel

CSMA 2011
10e Colloque National en Calcul des Structures
9-13 Mai 2011, Presqu'île de Giens (Var)

Coupling of finite element and boundary integral methods: Motion of ellipsoidal capsules in simple shear flow

A.V. Salsac[1], J. Walter[1,2], D. Barthès-Biesel[1]

[1] *Biomécanique et Bioingénierie (UMR CNRS 6600), Université de Technologie de Compiègne, email: a.salsac@utc.fr*
[2] *Present address: Chemical Engineering, University of California, Santa Barbara, USA*

Résumé — We introduce a novel numerical method to model the fluid-structure interaction between a microcapsule and an external flow. An explicit finite element method is used to model the large deformation of the capsule wall, which is treated as a bidimensional hyperelastic membrane. It is coupled with a boundary integral method to solve for the internal and external Stokes flows. The study aims at characterizing the motion and large deformation of an initially-ellipsoidal capsule subjected to a simple shear flow. Both oblate and prolate spheroids are considered. Two regimes are found depending on the value of the capillary number, ratio of the viscous to elastic forces. At low capillary number, the capsule tumbles, behaving mostly like a solid particle. At higher capillary numbers, the capsule has a fluid-like behavior. It oscillates in the shear plane, while its membrane continuously rotates around its deformed shape. During the tumbling-to-swinging transition, the capsule transits through an almost circular profile in the shear plane, for which a long axis can no longer be defined. Qualitatively, oblate and prolate capsules are found to behave similarly, particularly at large capillary numbers, when the influence of the initial state fades out. However, the capillary number at which the transition occurs is significantly lower for oblate spheroids.
Mots clés — fluid-structure interaction, finite element method, boundary integral method.

1 Introduction

Bioartificial capsules, which consist of an internal liquid protected by a thin hyperelastic wall, have many practical uses in pharmaceutical, cosmetic and bioengineering applications. They can also be seen as simplified models of red blood cells. When suspended in another flowing liquid, capsules undergo large deformations and strong fluid-structure viscous coupling due to the low-Reynolds-number flows of the internal and suspending liquids. The membrane mechanical behaviour has been extensively studied numerically for initially-spherical capsules in flow and different strategies have been considered to derive numerical solutions. Many studies have used a fluid solver based on the boundary integral method to solve for the Stokes flow equations (e.g. [1-5]). The velocity field at any position within the fluid domain is given by surface integrals calculated on the geometric boundaries. This method therefore has two main advantages : it reduces the geometric dimension of the problem by one, which largely decreases the total number of nodes, and avoids re-meshing the fluid domain at each time step, which is hugely costly.

The model the most used for the capsule wall is that of a 2D hyperelastic membrane : the wall is considered to be infinitely thin and to have a negligible bending stiffness. Two approaches may be considered to model the capsule membrane mechanics : the equations of the force equilibrium on the capsule wall may either be written locally at each point (strong form) or globally integrated over the capsule surface (weak form). Most capsule studies have used the strong form of the equations. Capsules in simple shear flows have been considered by Pozrikidis [1], Ramanujan & Pozrikidis [2] and more recently by Li & Sarkar [5], who computed the membrane load as a piecewise constant function. Lac *et al.* [3] and Lac & Barthès-Biesel [4] used instead bi-cubic B-splines as interpolation functions in order to compute the loads with high accuracy. These studies have shown that the capsule wall is dominated by in-plane membrane tensions, but compressive tensions can occur locally, creating wrinkles.

An alternative option is to write the balance equations in their weak form and to use a Finite Element (FE) method. The local equilibrium equations are converted into their variational equivalent. Eggleton & Popel [6] and Doddi & Bagchi [7] have coupled a FE method with an immersed boundary method. Ho-

wever their FE method, based on the use of linear (P1) elements, lacks generality in the implementation. The results are not very precise, which is probably a consequence of the method used for the fluids.

Recently, we have proposed a new method coupling the boundary integral method and the finite element method [8]. It has the advantage to use the same discretization for the fluids and capsule wall, which allows a Lagrangian tracking of the membrane position with high accuracy. The numerical stability and accuracy of the method have been demonstrated on a spherical capsule placed in different linear shear flows. The method has been shown to be very stable in the presence of in-plane compression.

Capsules with a non-spherical initial shape have been considered very little [9-11], even though they provide more realistic models of red blood cells. The extensive wrinkling that appear when such capsules deform had previously rendered most numerical simulations unstable. We presently study initially-ellipsoidal capsules placed in a simple shear flow such that their revolution axis is in the shear plane. We consider both oblate and prolate spheroids to characterize the influence of the capsule shape on the deformation. Particular attention will be paid to the regimes observed and to the transition between them.

2 Problem statement

We consider a spheroidal microcapsule of semi-axes denoted a along the revolution axis and b along the orthogonal directions. It consists of an infinitely thin membrane of surface shear elastic modulus G_s that encloses an incompressible liquid. It is suspended in a simple shear flow in the (x_1,x_2) plane :

$$\underline{v}^{\infty} = \dot{\gamma} x_2 \underline{e}_1, \tag{1}$$

where $\dot{\gamma}$ is the shear rate. The inner and outer fluids are supposed to be Newtonian and to have the same viscosity μ and density ρ. Two main parameters influence the capsule deformation. The capillary number

$$Ca = \frac{\mu \dot{\gamma} \ell}{G_s} \tag{2}$$

compares the viscous stresses in the flow to the elastic stresses in the membrane. The length scale ℓ is defined as the radius of the sphere having the same volume as the ellipsoid ($\ell = \sqrt[3]{ab^2}$). The other parameter is the aspect ratio a/b, ratio of the ellipsoid semi-axis lengthes. The spheroid is oblate when $a/b < 1$ and prolate when $a/b > 1$.

In the following sections, all studies are conducted for two initial values of the aspect ratio : $a/b = 0.5$ (oblate spheroid) and $a/b = 2$ (prolate spheroid). These two aspect ratios are well-suited to comparing the influence of the capsule initial shape. The two spheroids have, by definition, the same internal volume and therefore the same length scale, l. With initial surface areas differing by less than 2%, the two capsules essentially have the same initial value of the surface-area-to-volume ratio.

2.1 Membrane mechanics

Following [12], we treat the membrane as a purely bidimensional sheet of hyperelastic material. In particular, we neglect strain variations across the thickness and therefore the bending stiffness of the material. We introduce the displacement $\underline{U}(\underline{X},t) = \underline{x}(\underline{X},t) - \underline{X}$, where $\underline{X}$ and $\underline{x}$ are the positions of a given material point in the reference and deformed state. It is related to the velocity of the membrane through the kinematic condition :

$$\frac{\partial}{\partial t}\underline{U}(\underline{X},t) = \underline{v}(\underline{x},t)\,. \tag{3}$$

The numerical procedure consists in following the position of the capsule membrane after the start of flow. At each time step, the membrane deformation is thus known : it is quantified by the principal dilation ratios λ_1 and λ_2 in its plane. Two deformation invariants are generally used :

$$I_1 = \lambda_1^2 + \lambda_2^2 - 2, \quad I_2 = \lambda_1^2\lambda_2^2 - 1 = J_s^2 - 1. \tag{4}$$

The Jacobian $J_s = \lambda_1\lambda_2$ represents the ratio of the deformed to the undeformed surface areas.

Elastic stresses in an infinitely thin membrane are replaced by the elastic tensions corresponding to forces per unit arc length measured in the plane of the membrane. When the membrane is a two-dimensional isotropic material, the Cauchy tension tensor $\underline{\underline{\tau}}$ can be related to a strain energy function

per unit area of undeformed membrane $w_s(I_1, I_2)$. Presently we will consider two hyperelastic laws. The neo-Hookean law describes the behaviour of an infinitely thin sheet of a three-dimensional isotropic material

$$w_s^{NH} = \frac{G_s}{2}\left(I_1 - 1 + \frac{1}{I_2+1}\right). \tag{5}$$

The area dilation modulus is then $K_s = 3G_s$. Skalak *et al.* [12] derived a constitutive law for two-dimensional materials with independent surface shear and area dilation moduli

$$w_s^{Sk} = \frac{G_s}{4}\left(I_1^2 + 2I_1 - 2I_2 + CI_2^2\right), \quad C > -1/2. \tag{6}$$

The area dilation modulus is then $K_s = G_s(1+2C)$ and the Poisson ratio $\nu_s = C/(1+C)$. The Sk law was initially designed to model the area-incompressible membrane of biological cells, such as red blood cells, corresponding to $C \gg 1$.

The finite element method is then used to solve the equilibrium of the membrane

$$\nabla_s \cdot \underline{\underline{\tau}} + \underline{q} = \underline{0}. \tag{7}$$

where $\underline{q}$ is the unknown viscous load exerted by the fluids on the membrane and $\nabla_s\cdot$ the surface divergence operator in the deformed configuration. The local equilibrium is written in a weak form using the virtual work principle. Let $\mathcal{V}$ be the Sobolev space H^1. For any virtual displacement field $\underline{\hat{u}} \in \mathcal{V}$, the internal and external virtual work balance requires

$$\int_S \underline{\hat{u}} \cdot \underline{q}\, dS - \int_S \underline{\underline{\hat{\varepsilon}}}(\underline{\hat{u}}) : \underline{\underline{\tau}}\, dS = 0, \tag{8}$$

where $\underline{\underline{\hat{\varepsilon}}}(\underline{\hat{u}}) = \frac{1}{2}\left(\nabla_s \underline{\hat{u}} + \nabla_s \underline{\hat{u}}^T\right)$ is the virtual strain tensor. The equation is solved for the load $\underline{q}$. Note that most finite element procedures look instead for the displacement field, treating the forces as known. This is not possible when dealing with a capsule : the lack of kinematic boundary conditions implies that the displacement solution is not unique.

2.2 Internal and external flows

Once the load $\underline{q}$ is known, the velocity field can be calculated solving for the internal and external flows with the boundary integral method. The flows are indeed governed by the Stokes equations, as the Reynolds number $Re = \rho l^2 \dot{\gamma}/\mu$ is infinitely small. To determine the new position of the capsule at the following time step, one needs to solve for the velocity of the points of the capsule. The latter can be expressed as an integral equation over the deformed capsule surface S :

$$\forall \underline{x}_0 \in S, \quad \underline{v}(\underline{x}_0) = \underline{v}^\infty(\underline{x}_0) + \frac{1}{8\pi\mu}\int_S \underline{\underline{J}}(\underline{x}_0, \underline{x}) \cdot \underline{q}(\underline{x})\, dS, \tag{9}$$

where $\underline{v}^\infty$ is the undisturbed flow velocity, $\underline{\underline{J}}$ is the Green's single layer kernel, $\underline{r} = \underline{x}_0 - \underline{x}$ and $r = \|\underline{r}\|$. The new position of the membrane points is obtained solving (3).

2.3 Numerical method

For a given deformed state of the capsule, we first solve the solid problem (8). $\mathcal{V}$ is discretized as a finite element space using an unstructured mesh, with quadratic (P_2) curved triangular elements. The discretized problem leads to the following matrix system :

$$[M]\{q^N\} = \{R\}, \tag{10}$$

where $\{q^N\}$ corresponds to the degrees of freedom of the discretized load, $[M]$ has the structure of a mass matrix and $\{R\}$ corresponds to the right-hand side of (8) and depends non-linearly on the displacement $\underline{U}$. The tensions $\underline{\underline{\tau}}$ are computed directly using the strain energy function w_s. Solving the solid problem consists in assembling $\{R\}$ and $[M]$ on the deformed state. Surface integration is performed using Hammer points on the elements. Eq. (10) is then solved using the sparse solver Pardiso [13].

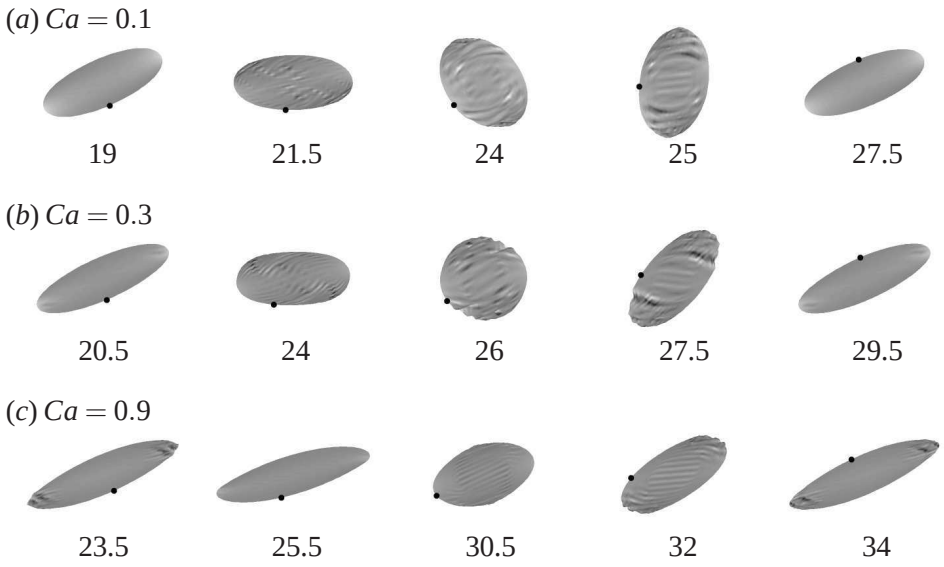

FIGURE 1 – Evolution of the capsule shape in the shear plane over one half period. The initial shape is a prolate spheroid, $a/b = 2$, and the membrane follows the Sk law with $C = 1$. The grey scale corresponds to the normal component of the load, $\underline{q} \cdot \underline{n}$. The dot shows the position of material point P, originally on the short axis. The value of the non-dimensional time step $\dot{\gamma}t$ is given below each shape.

The velocity field is obtained explicitly from the boundary integral equation (9), which is discretized on the *same mesh* as for the solid problem, once again using Hammer points for the integration. Finally, the new position is obtained by convecting the nodes after integrating (3) numerically with a second-order Runge-Kutta method. More information on the convergence and stability of the method may be found in [8].

3 Results

3.1 Motion modes : tumbling and swinging

Depending on the value of the capillary number Ca, a given ellipsoidal capsule may exhibit two types of motion. At low flow strength, a "solid-like" regime occurs, called *tumbling*. Oblate and prolate spheroids exhibit a similar behaviour. Figure 1(a) shows the time evolution of a prolate ellipsoidal capsule with initial aspect ratio $a/b = 2$ ($a/\ell = 1.59$) and a Sk membrane ($C = 1$) for $Ca = 0.1$. It shows that, during tumbling, the capsule rotates like a quasi-rigid ellipsoid subjected to the flow vorticity, while the internal flow is almost stationary with respect to the membrane. This is illustrated by the fact that point P that was initially on the small axis of the ellipsoid, remains in the vicinity of its initial location.

Since the capsule profile may be quite difficult to characterize, we evaluate the capsule distortion by the deformation of its ellipsoid of inertia [2]. This method is widely used, but gives approximate results when the deformed particle shape is far from ellipsoidal. By symmetry, the material points initially located in the shear plane (x_1, x_2) remain in it and two of the principal axes of the ellipsoid of inertia with semi-axes L_1 and L_2 ($L_1 \geq L_2$) are also located in the shear plane. Correspondingly, it is convenient to quantify the three-dimensional capsule deformation with the deformation of the intersection of the profile with the shear plane. The Taylor deformation parameter is then defined as

$$D_{12} = \frac{L_1 - L_2}{L_1 + L_2}. \tag{11}$$

Note that, contrary to a spherical capsule, the initial value of D_{12} is not zero and is given by $D_{12}^0 = |a - b|/(a + b)$. The time-evolution of the Taylor parameter D_{12} is shown in figure 2a. The large oscillations prove that the membrane can undergo large displacements without large deformation, which is due to the initial shape flaccidity (measured by the surface area to volume ratio).

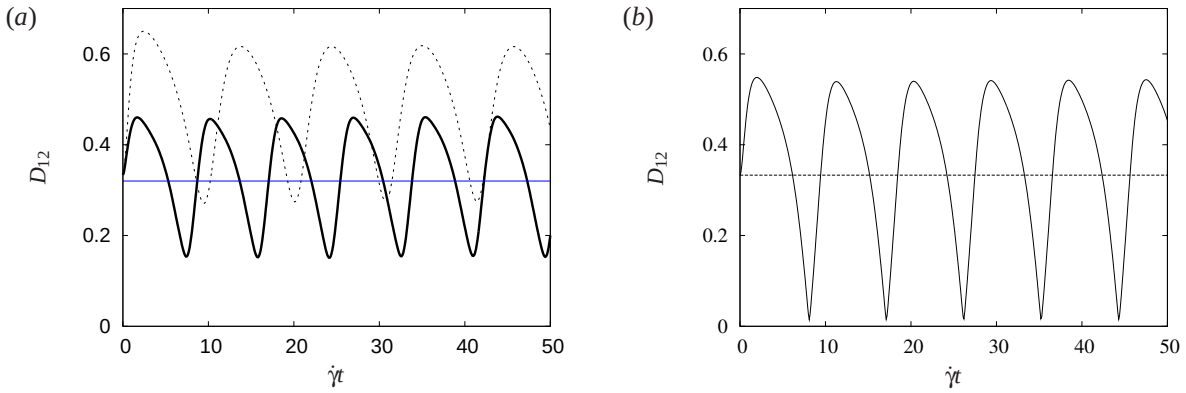

FIGURE 2 – Taylor parameter D_{12} as a function of time. (*a*) solid line : Sk law $C = 1$, $a/b = 2$, $Ca = 0.1$ (tumbling regime), dotted line : Sk law $C = 1$, $a/b = 2$, $Ca = 0.9$ (swinging regime), horizontal line : $D_{12}^0 = 0.33$ (*b*) Sk law $C = 1$, $a/b = 2$, $Ca = 0.9$ (transition).

At higher flow strength, a "fluid-like" regime occurs, called *swinging*. The membrane rotates around the deformed shape of the capsule similarly to the tank-treading motion observed for spherical capsules. Because of the initial anisotropy of the reference shape, the membrane points are not equivalent : a stationary steady state is not possible and a periodic motion of the deformed capsule occurs. Like in the tumbling regime, oblate and prolate spheroids behave similarly in the swinging regime. We illustrate the salient motion features for the same ellipsoidal capsule at $Ca = 0.9$ (fig. 1*c*). The capsule assumes an elongated shape with a long axis aligned with the maximum flow strain direction, while the membrane continuously rotates around the deformed shape. The time evolution of the Taylor parameter D_{12} is also shown in figure 2*a*. It can be noted that D_{12} oscillates around a mean value that is larger than in the tumbling regime. The capsule reaches its maximum deformation, when the material points located originally on the longer axis of the ellipsoid are in the straining direction (see fig. 1*c*, $\dot{\gamma}t = 23.5$). Conversely, D_{12} is minimum when the points originally on the smaller axis are in the straining direction, or equivalently, when the points originally on the longer axis are aligned with the flow compression direction ($\dot{\gamma}t = 30.5$).

3.2 Tumbling-swinging transition

In order to study the tumbling-to-swinging transition, we consider the same capsule ($a/b = 2$) at a capillary number $Ca = 0.3$. One characteristic difference between the tumbling and swinging regimes is the time-evolution of the capsule long axis. In the tumbling regime, the long axis rotates over time, while it oscillates around a mean value in the swinging regime. This is how the transition has been previously defined [9-11]. However, we believe that such a criterion is not quite appropriate to determine the critical capillary number $Ca^\star$ at which the transition occurs. Indeed, figure 1(*b*) shows that during each half-cycle, the capsule transits through an almost circular profile in the shear plane (here at $\dot{\gamma}t = 26$). At this time, the two principal axes of the ellipsoid of inertia in the shear plane have roughly the same length ($L_1 \approx L_2$), thus there is no clearly identified "long" axis. The fact that the capsule profile becomes quasi circular in the shear plane shows that the transition corresponds to a Taylor parameter getting close to zero at its minimum (figure 2(*b*). In conclusion, we propose to define the critical capillary number $Ca^\star$ as an interval using the criterion

$$\min D_{12} < 0.05\,, \tag{12}$$

$\min D_{12}$ being the minimum value of the Taylor parameter over one period. This criterion corresponds to a relative difference of 10% between the lengths L_1 and L_2 of the axes, which is the minimum difference that can be quantified with precision.

Figure 1 also shows that the transition is associated with an increased wrinkling of the capsule wall. The most extensive wrinkling is seen to occur as D_{12} approaches 0, i.e. as the long axis of the undeformed ellipsoid becomes shorter. However, wrinkling is transient during the cycle and the wrinkles disappear when the capsule long axis is in the direction of the viscous stretch ($\dot{\gamma}t = 20.5$ in figure 1*b*).

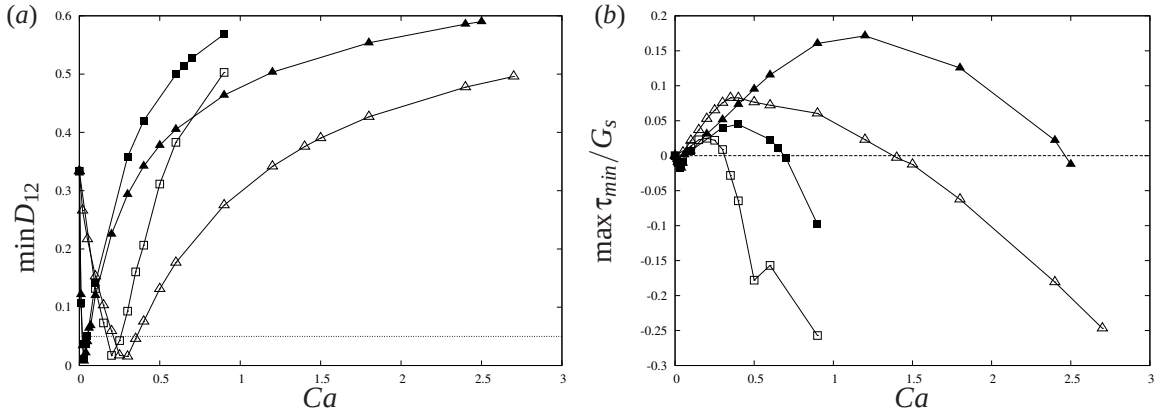

FIGURE 3 – (*a*) Minimum values of the Taylor parameter D_{12} of the ellipsoid of inertia. The horizontal line corresponds to the limit $\min D_{12} = 0.05$ used to define the transition. (*b*) Maximum value during a period of the minimum principal tension. Results are shown for an oblate spheroid ($a/b = 0.5$, filled symbols) and a prolate spheroid ($a/b = 2$, open symbols). □ : NH law ; △ : Sk law with $C = 1$.

3.3 Effect of capillary number

We now conduct a systematic study of the motion of a spheroidal capsule in a simple shear flow as a function of the capillary number. Two material laws are used to describe the membrane, the neo-Hookean law (5) and Skalak's law (6) with $C = 1$, which have the same behaviour at small deformation. Two initial aspect ratios are studied : $a/b = 0.5$ and $a/b = 2$. This makes it possible to compare the behaviour of oblate and prolate spheroids, but a systematic study of the influence of the aspect ratio is outside the scope of this article.

The minimum value $\min D_{12}$ is shown as a function of Ca and membrane law in figure 3*a*. A larger value of Ca is required to reach the same value of D_{12} with the Sk law than with the NH law. If the NH and Sk ($C = 1$) laws behave similarly at small deformation levels, they are known to diverge at larger deformation, the Sk law exhibiting a strain-hardening behaviour and the NH law a strain-softening one.

Figure 3*a* also proves that $\min D_{12}$ indeed goes through a global minimum in all cases. The criterion $\min D_{12} < 0.05$ provides values of $Ca^\star$ confined within a small interval, because of the sharp variations of $\min D_{12}$ around the global minimum. To determine the intervals for the critical capillary number $Ca^\star$, the capillary number was increased systematically by steps of 0.01 for oblate spheroids and 0.05 for prolate spheroids. The values of capillary number for which $\min D_{12} < 0.05$ are provided in table 1. Note that, for a given aspect ratio, the $Ca^\star$ intervals are almost equal for the two material laws considered. This is due to the fact that the transition takes place at moderate deformation levels, for which the two laws behave similarly. However, oblate and prolate capsules have values of $Ca^\star$ that differ by a factor ~ 10. As the 2 capsules studied ($a/b = 0.5, 2$) share the same initial value for the Taylor parameter in the shear plane ($D_{12}^0 = 0.33$), any difference in their behaviour is due to the difference in their initial geometry in the orthogonal direction. The prolate ellipsoidal capsule therefore requires a higher energy to reach the shape for which $D_{12} \sim 0$ than an oblate capsule, because of its short characteristic length in the orthogonal direction.

It is shown in figure 1 that widespread in-plane compression can occur. In the absence of a physical bending stiffness in the numerical model, such compressive tensions cause numerical wrinkles. In order to study in-plane compression, figure 3*b* shows the maximum value over one period of $\tau_{min}(t)$, the minimum principal tension, denoted $\max \tau_{min}$:

$$\max \tau_{min} = \max_t \left(\tau_{min}(t)\right) = \max_t \left(\min_{\underline{x}, i=1,2} \left(\tau_i(\underline{x}, t)\right) \right), \tag{13}$$

where τ_i are the principal tensions. In all the cases studied, τ_{min} is negative through most of the period indicating that compression always occurs somewhere for spheroidal capsules. The positive values of τ_{min} occur when the long axis of the original ellipsoid is in the straining direction.

Figure 3*b* shows that, for large values of Ca, even the maximum value of τ_{min} is negative. It means

	$a/b = 0.5$	$a/b = 1$	$a/b = 2$
NH	$Ca^\star \in [0.02, 0.04]$	$\star$	$Ca^\star \in [0.20, 0.25]$
	$Ca_H = 0.70$	$Ca_H = 0.63$	$Ca_H = 0.35$
Sk, $C = 1$	$Ca^\star \in [0.02, 0.05]$	$\star$	$Ca^\star \in [0.25, 0.35]$
	$Ca_H = 2.5$	$Ca_H = 2.4$	$Ca_H = 1.4$

TABLE 1 – Values of the critical capillary numbers $Ca^\star$ and Ca_H for the cases studied. The values of Ca_H are provided for an initially-spherical capsule for reference [3].

that negative tensions occur even when the capsule reaches its maximum elongation. The reason is that, at large values of Ca, negative tensions and wrinkles appear at the tips of the elongated capsule. Lac *et al.* [3] observed this phenomenon for an initially-spherical capsule ($a/b = 1$) and defined Ca_H as the capillary number above which negative tensions appear at steady state. In the case of spheroidal capsules, we define Ca_H as the critical capillary number above which $\max \tau_{min} < 0$. The values of Ca_H found for the different cases studied are provided in table 1.

Except for a prolate NH spheroid, the largest amount of wrinkling occurs in the swinging regime, for values of Ca slightly above $Ca^\star$. During tank-treading motion, strong wrinkling tends to occur when the long axis of the initial ellipsoid has to be compressed to become the short axis of the deformed capsule. However, as the capillary number is increased and the capsule becomes more elongated, the isotropic component of the tensions (related to the Poisson ratio of the membrane) increases and compensates the negative tensions : wrinkling becomes less important. The maximum amount of wrinkling therefore occurs during transition and for capillary numbers slightly above it.

In the case of a prolate NH spheroid, the wrinkling does not subside as Ca increases. This is a consequence of the proximity of the two critical capillary numbers $Ca^\star \in [0.20, 0.25]$ and $Ca_H = 0.35$ in this particular case. Indeed, if we consider a material point originally on the long axis of the ellipsoid, at $Ca \approx 0.35$ the point is on the short axis of the deformed capsule and strong wrinkling occurs, since Ca is only slightly above $Ca^\star$. A quarter of a period later, the material point is in the straining direction, but buckling and wrinkling occur at the tips, as Ca is around Ca_H. These two phenomena then lead to a constant wrinkling of the membrane, that even seems to amplify over time, but this is probably a numerical artifact due to the lack of a proper bending stiffness in the model of the capsule wall.

4 Conclusion

We have modelled the behaviour and large deformation of an ellipsoidal capsule in a simple shear flow using the novel method of Walter *et al.* [8], that couples boundary integrals for the flows to finite membrane elements. The study has shown that the coupling method is well-suited to the simulation of non-spherical capsules and that it remains numerically stable in the presence of in-plane compression, even though the mechanical wall model does not account for bending stiffness. This is a convenient feature when the bending effects remain localised and weak. Still, to model exactly the physical behaviour of the capsule wall, a proper shell model remains to be implemented.

The coupling method allowed us to study the behaviour of oblate and prolate spheroids, with aspect ratios $a/b = 0.5$ and $a/b = 2$, and to recognise two regimes : a quasi-solid regime ('tumbling') at low capillary numbers, where the long axis of the capsule rotates in the shear plane, and a quasi-fluid regime ('swinging') at high capillary numbers, where this axis oscillates around a mean inclination and membrane rotation (tank treading) occurs. These two regimes are separated by a transition region, during which the capsule transits through a phase where the two axes of the capsule in the shear plane are approximately of the same length ($D_{12} \approx 0$). For the transition to occur, the critical stage is for the points initially located on the small axis to have enough energy to pass the long axis of the deformed capsule. The transition can thus be understood as the crossing of an energy barrier as proposed by Skotheim & Secomb [14]. However, in their semi-analytical theory, they supposed that the shape of the capsules remained constant and postulated a periodic variation of the strain energy of the membrane. The present study shows that the capsule shape changes over time and that the energy variation is thus more complex than predicted.

We have also shown that oblate and prolate spheroids behave qualitatively similarly in most respects. Still the capsule initial shape influences the transition between the tumbling and swinging regimes, which occurs at a much lower value of Ca for oblate spheroids. The tumbling regime is therefore limited to a very small range of capillary numbers for oblate spheroids, as the value of the critical capillary number at transition is low.

We do not believe that the transition can be considered as a separate regime, distinct from tumbling and swinging. It rather corresponds to the parameter range where the two regimes behave so closely that they cannot be accurately distinguished from one another. Along with the present study, all the existing numerical studies of capsules in simple shear flow indicate that the tumbling-to-swinging transition is associated with a phase when $D_{12} \approx 0$ [9, 10, 11]. A similar behaviour has been found experimentally for lipid vesicles [15, 16]. These findings are, however, at odds with the experiments conducted by Abkarian *et al.* [17] on red blood cells in a simple shear flow. They observe that, during the tumbling-to-swinging transition, the red blood cell maintains an almost constant shape and that the transition occurs through an *intermittent regime* during which the cell alternately swings and tumbles. However, our study and the other numerical studies cited above fail to find such an intermittent regime and always observe that the tumbling-to-swinging transition is associated with large variations of the capsule shape.

Références

[1] C. Pozrikidis. *Finite deformation of liquid capsules enclosed by elastic membranes in simple shear flow.* J. Fluid Mech., 297, 123–152, 1995.

[2] S. Ramanujan, C. Pozrikidis. *Deformation of liquid capsules enclosed by elastic membranes in simple shear flow : Large deformations and the effect of capsule viscosity.* J. Fluid Mech., 361, 117–143, 1998.

[3] É. Lac, D. Barthès-Biesel, N. A. Pelekasis, J. Tsamopoulos. *Spherical capsules in three-dimensional unbounded Stokes flow : effect of the membrane constitutive law and onset of buckling.* J. Fluid Mech., 516, 303–334, 2004.

[4] É. Lac, D. Barthès-Biesel. *Deformation of a capsule in simple shear flow : effect of membrane prestress.* Phys. Fluids, 17, 0721051–0721058, 2005.

[5] X. Li, K. Sarkar. *Front tracking simulation of deformation and buckling instability of a liquid capsule enclosed by an elastic membrane.* J. Comp. Phys., 227, 4998–5018, 2008.

[6] C. D. Eggleton, A. S. Popel. *Large deformation of red blood cell ghosts in a simple shear flow.* Phys. Fluids, 10, 1834–1845, 1998.

[7] S.K. Doddi, P. Bagchi. *Lateral migration of a capsule in a plane Poiseuille flow in a channel.* Int. J. Multiphase Flow, 34, 966–986, 2008.

[8] J. Walter, A.-V. Salsac, D. Barthès-Biesel, P. Le Tallec. *Coupling of finite element and boundary integral methods for a capsule in a Stokes flow.* Int. J. Num. Meth. Engng, 83, 829–850, 2010.

[9] S. Kessler, R. Finken, U. Seifert. *Swinging and tumbling of elastic capsules in shear flow.* J. Fluid Mech., 605, 207–226, 2008.

[10] Y. Sui, H.T. Low, Y.T. Chew, P. Roy. *Swinging and tumbling of elastic capsules in shear flow.* Phys. Rev. E, 77, 016310, 2008.

[11] P. Bagchi, R. M. Kalluri. *Dynamics of nonspherical capsules in shear flow.* Phys. Rev. E, 80, 016307, 2009.

[12] R. Skalak, A. Tozeren, R. P. Zarda, S. Chien. *Strain energy function of red blood cell membranes.* Biophys. J., 13, 245–264, 1973.

[13] O. Schenk, K. Gärtner. *Solving unsymmetric sparse systems of linear equations with PARDISO.* Future Generation Computer Systems, 20, 475–487, 2004.

[14] J.M. Skotheim, T.W. Secomb. *Red Blood Cells and Other Nonspherical Capsules in Shear Flow : Oscillatory Dynamics and the Tank-Treading-to-Tumbling Transition.* Phys. Rev. Lett., 98, 078301, 2007.

[15] V. Kantsler, V. Steinberg. *Transition to Tumbling and Two Regimes of Tumbling Motion of a Vesicle in Shear Flow.* Phys. Rev. Lett., 96, 036001, 2006.

[16] J. Deschamps, V. Kantsler, V. Steinberg. *Phase Diagram of Single Vesicle Dynamical States in Shear Flow.* Phys. Rev. Lett., 102, 118105, 2010.

[17] M. Abkarian, M. Faivre, A. Viallat. *Swinging of Red Blood Cells under Shear Flow.* Phys. Rev. Lett., 98, 188302, 2007.